

# Numerical Simulation of High Mach Number Astrophysical Jets with Radiative Cooling

Youngsoo Ha,<sup>1</sup> Carl L. Gardner,<sup>2</sup> Anne Gelb,<sup>2</sup> and Chi-Wang Shu<sup>3</sup>

*Received October 21, 2003; accepted (in revised form) January 29, 2004*

---

Computational fluid dynamics simulations using the WENO-LF method are applied to high Mach number nonrelativistic astrophysical jets, including the effects of radiative cooling. Our numerical methods have allowed us to simulate astrophysical jets at much higher Mach numbers than have been attained (Mach 20) in the literature. Our simulations of the HH 1-2 astrophysical jets are at Mach 80. Simulations at high Mach numbers and with radiative cooling are essential for achieving detailed agreement with the astrophysical images.

---

**KEY WORDS:** astrophysical jets; radiative cooling; WENO method

## 1. INTRODUCTION

Hubble Space Telescope images have revealed a new wealth of detail in gas flows and shock wave patterns involving astrophysical jets and colliding interstellar winds of particles. Simulating the fluid flows and shock wave patterns and detailed temperature profiles by implementing theoretical models in a gas dynamics simulator will help in analyzing the processes at work in these astrophysical objects. In this investigation we apply the WENO-LF method [1]—a modern high-order upwind method—to simulate high Mach number nonrelativistic astrophysical jets from young stars including the effects of radiative cooling. In the astrophysical setting, the jet gas is on the order of ten times the density of the ambient gas. Simulations at high Mach numbers and with radiative cooling are essential

---

<sup>1</sup> Division of Applied Mathematics, Korean Advanced Institute of Science and Technology, Taejon 305-701, South Korea. E-mail: youngsooha@kaist.ac.kr

<sup>2</sup> Department of Mathematics and Statistics, Arizona State University, Tempe, AZ 85287-1804, USA. E-mails: {gardner,ag}@math.asu.edu

<sup>3</sup> Division of Applied Mathematics, Brown University, Providence, RI 02912, USA. E-mail: shu@dam.brown.edu

for achieving detailed agreement with the astrophysical observations. For example, the gas flows in the HH 1–2 astrophysical jets are at about Mach 80. The WENO-LF method allows us to simulate astrophysical jets at much higher Mach numbers than have been attained in the literature. The wide range of supersonic jets simulated by Norman *et al.* [2,3] have Mach numbers in the range 1.5–12, while the maximum Mach number of the jets simulated by Norman and Stone [4–8] is 20. Our simulations of the HH 1–2 astrophysical jets are at Mach 80. (The convention is to specify the Mach number of the jet with respect to the jet gas.)

Other early supersonic jet simulations were done in [9,10] using the front-tracking method. Instabilities and asymmetries of astrophysical jets are treated by Norman [11,12] and by Stone *et al.* in [13–15], including radiative cooling. Recent astrophysical jet simulations emphasizing three-dimensional computations and relativistic jets (still at Mach numbers  $\leq 20$ ) are summarized by Müller [16].

We will apply the WENO-LF simulations in modeling the detailed astrophysical gas flows imaged by the Hubble Space Telescope, like the image of the pair of astrophysical jets HH 1–2 by Hester *et al.* [17], which depicts shock waves including strong bow and terminal shocks, Kelvin–Helmholtz rollup of the jet tips, and interaction of the jets with their ambient environment.

Computer simulations and astrophysical theory will allow us to analyze the detailed properties of astrophysical jet flows: Can we model and understand the shock waves that develop in and around the jet? What are the temperatures, densities, velocities, and chemical compositions of the jets? How do radiative cooling of the jet gas and interaction of the jet with inhomogeneities in the ambient environment affect morphology and propagation?

Here we describe our implementation of the two-dimensional “slab” jet problem using the WENO-LF method, including a realistic model for radiative cooling. The simulations of the basic jet flows agree well with the Hubble Space Telescope images of HH 1–2.

## 2. GAS DYNAMICS WITH RADIATIVE COOLING

The equations of gas dynamics take the form

$$\frac{\partial \rho}{\partial t} + \frac{\partial}{\partial x_i}(\rho u_i) = 0, \quad (1)$$

$$\frac{\partial}{\partial t}(\rho u_j) + \frac{\partial}{\partial x_i}(\rho u_i u_j) + \frac{\partial P}{\partial x_j} = 0, \quad (2)$$

$$\frac{\partial E}{\partial t} + \frac{\partial}{\partial x_i}(u_i(E + P)) = -n^2 \Lambda(T), \quad (3)$$

where  $\rho = m_H n$  is the density of the the gas (predominantly H),  $m_H = 938.272 \text{ MeV}/c^2$  is the mass of H,  $n$  is the number density,  $u_i$  is the velocity,  $\rho u_i$  is the momentum density,  $P = nk_B T$  is the pressure,  $k_B$  is Boltzmann's constant<sup>1</sup>,  $T$  is the temperature, and

$$E = \frac{3}{2}nk_B T + \frac{1}{2}\rho u^2 \quad (4)$$

is the energy density. Indices  $i, j$  equal 1, 2, 3, and repeated indices are summed over. The pressure is related to the internal energy density by the equation of state, which to an excellent approximation is polytropic:

$$P = (\gamma - 1) \left( E - \frac{1}{2}\rho u^2 \right), \quad (5)$$

where the polytropic gas constant  $\gamma = 5/3$  for a monatomic gas like H.

Radiative cooling of the gas is incorporated through the right-hand side of Eq. (3), with the model for  $\Lambda(T)$  taken from Fig. 8 of [18]. The cooling law can be modeled approximately by

$$\left( \frac{dE}{dt} \right)_{\text{cooling}} = -n^2 \Lambda(T) \approx \begin{cases} -\tilde{\Lambda}(P^2 - P_a^2), & T > T_a, \\ 0, & \text{otherwise,} \end{cases} \quad (6)$$

where  $\tilde{\Lambda} = 8.776$  in our computational units,  $P_a$  is the ambient pressure, and  $T_a$  is the ambient temperature. The approximation (6) begins to break down for  $T > T_* \sim 10^6 \text{ K}$ .

### 3. NUMERICAL METHODS

We use a third-order WENO-LF [1] (weighted essentially nonoscillatory Lax-Friedrichs) finite difference method for our supersonic astrophysical flow simulations. We have extended and adapted the code for simulating very high Mach number flows with radiative cooling.

ENO and WENO schemes are high-order finite difference schemes designed for nonlinear hyperbolic conservation laws with piecewise smooth solutions containing sharp discontinuities like shock waves and contacts. Locally smooth stencils are chosen via a nonlinear adaptive algorithm to avoid crossing discontinuities whenever possible in the interpolation procedure. The weighted ENO schemes use a convex combination of all candidate stencils, rather than just one as in the original ENO method.

---

<sup>1</sup> $k_B$  can be set equal to 1 if  $T$  is measured in energy units, with the correspondence  $1 \text{ eV} = 11,604.4 \text{ K}$ .

We tried two different methods of incorporating the radiative cooling source term in the gas dynamics equations: a splitting method (for CLAW-PACK and for an implicit treatment of cooling in WENO-LF), and (2) an unsplit method for WENO-LF with an explicit treatment of cooling. The computational results were virtually identical. In the splitting method, first we solve the homogeneous gas dynamics equations (with  $\Lambda \equiv 0$ ), and then we update the energy density  $E$  by solving the ordinary differential equation (ODE)

$$\frac{dE}{dt} = -n^2 \Lambda(T) \quad (7)$$

with the initial condition for  $E$  given by the results from the first step. In the splitting method only the energy density  $E$  is changed in the cooling partial step, while  $\rho$  and  $\mathbf{u}$  are held fixed. The ODE is solved using either an explicit third-order Runge–Kutta method or an implicit second-order trapezoidal rule method (which guarantees stability even for very large timesteps). In the unsplit method in WENO-LF, the cooling term is simply added in on the right-hand side of the explicit third-order Runge–Kutta method.

We now describe the computational procedure for the third-order WENO scheme in more detail. Spatial discretization is discussed first. We start with the simple case of a scalar equation

$$u_t + f(u)_x = 0 \quad (8)$$

and assume  $\partial f(u)/\partial u \geq 0$ , i.e., that the “wind direction” is positive. More general cases will be described later. The computational domain is discretized into a uniform mesh of  $N$  gridpoints  $x_i = i\Delta x$ ,  $i = 1, 2, \dots, N$ , where  $\Delta x$  is the uniform mesh size. A smooth nonuniform mesh could also be used to concentrate gridpoints in certain regions to obtain better resolution. A conservative numerical approximation  $u_j(t)$  to the exact solution  $u(x_j, t)$  of (8) satisfies the following ODE system:

$$\frac{du_j(t)}{dt} + \frac{1}{\Delta x} \left( \hat{f}_{j+1/2} - \hat{f}_{j-1/2} \right) = 0, \quad (9)$$

where  $\hat{f}_{j+1/2}$  is called the numerical flux, the design of which is the key ingredient for a successful scheme. For the third-order WENO scheme, the numerical flux  $\hat{f}_{j+1/2}$  is defined as follows:

$$\hat{f}_{j+1/2} = \omega_1 \hat{f}_{j+1/2}^{(1)} + \omega_2 \hat{f}_{j+1/2}^{(2)}, \quad (10)$$

where  $\hat{f}_{j+1/2}^{(m)}$ , for  $m=1, 2$ , are the two second-order accurate fluxes on two different stencils given by

$$\hat{f}_{j+1/2}^{(1)} = -\frac{1}{2}f_{j-1} + \frac{3}{2}f_j, \quad \hat{f}_{j+1/2}^{(2)} = \frac{1}{2}f_j + \frac{1}{2}f_{j+1}. \quad (11)$$

The nonlinear weights  $\omega_m$  are given by

$$\omega_m = \frac{\tilde{\omega}_m}{\sum_{l=1}^2 \tilde{\omega}_l}, \quad \tilde{\omega}_l = \frac{\gamma_l}{(\varepsilon + \beta_l)^2} \quad (12)$$

with the linear weights  $\gamma_l$  given by

$$\gamma_1 = \frac{1}{3}, \quad \gamma_2 = \frac{2}{3} \quad (13)$$

and the smoothness indicators  $\beta_l$  by

$$\beta_1 = (f_j - f_{j-1})^2, \quad \beta_2 = (f_{j+1} - f_j)^2. \quad (14)$$

Finally, the parameter  $\varepsilon$  insures that the denominator in Eq. (12) never becomes 0, and is fixed at  $\varepsilon = 10^{-6}$  in the computations presented here. The choice of  $\varepsilon$  does not affect accuracy: the numerical errors can be much lower than  $\varepsilon$ , approaching machine zero. Note that we have used the short-hand notation  $f_j$  to denote  $f(u_j(t))$ , and that the stencil for the scheme is biased to the left because of the positive wind direction.

This completes the description of the third-order finite difference WENO scheme [19,20] for the scalar equation with a positive wind direction. As we can see, the algorithm is actually quite simple and there are no parameters to be tuned in the scheme. The main reason that it works well, both for smooth solutions and for solutions containing shocks or other discontinuities or high gradient regions, is that the nonlinear weights, determined by the smoothness indicators, automatically adjust themselves based on the numerical solution to use the locally smoothest information given by the solution. Higher order WENO schemes are available along the same lines [20–22].

If the wind direction  $\partial f(u)/\partial u \leq 0$ , the method for computing the numerical flux  $\hat{f}_{j+1/2}$  is the exact mirror image with respect to the point  $x_{j+1/2}$  of the description above. The stencil would then be biased to the right. If  $\partial f(u)/\partial u$  changes sign, we use a smooth flux splitting

$$f(u) = f^+(u) + f^-(u), \quad (15)$$

where  $\partial f^+(u)/\partial u \geq 0$  and  $\partial f^-(u)/\partial u \leq 0$ , and apply the above procedure separately on each of them. There are many choices of such flux splittings; the most popular one is the Lax–Friedrichs flux splitting where

$$f^\pm(u) = \frac{1}{2} (f(u) \pm \alpha u) \quad (16)$$

with  $\alpha = \max_u |\partial f(u)/\partial u|$ .

For hyperbolic systems of conservation laws (8), the eigenvalues of the Jacobian  $\partial f(u)/\partial u$  are all real, and there is a complete set of right and left eigenvectors. This allows us to apply the nonlinear WENO procedure in each of the local characteristic fields, obtained by using the left eigenvectors of the Jacobian. For multiple spatial dimensions, the finite difference version of WENO schemes simply applies the WENO procedure in each direction to obtain high order approximations to the relevant spatial derivatives. Unlike dimensional splitting, such a dimension by dimension method allows us to obtain high order accuracy without the computational cost of truly multidimensional reconstructions. For details, see [20,22].

The time discretization is implemented by a third-order TVD Runge–Kutta method [23]:

$$\begin{aligned} u^{(1)} &= u^n + \Delta t L(u^n, t^n), \\ u^{(2)} &= \frac{3}{4}u^n + \frac{1}{4}u^{(1)} + \frac{1}{4}\Delta t L(u^{(1)}, t^n + \Delta t), \\ u^{n+1} &= \frac{1}{3}u^n + \frac{2}{3}u^{(2)} + \frac{2}{3}\Delta t L(u^{(2)}, t^n + \frac{1}{2}\Delta t), \end{aligned} \quad (17)$$

where  $L$  is the approximation of the spatial derivatives  $L(u, t) \approx -\partial f(u)/\partial x$  by the WENO procedure outlined above. The time discretization is stable if the first-order forward Euler timestepping of the spatial operator is stable (see [24] for more details). This time discretization is very simple and consists of convex combinations of three first-order forward Euler steps. A CFL condition is needed for stability:

$$\alpha \frac{\Delta t}{\Delta x} \leq \text{CFL}, \quad (18)$$

where  $\alpha$  should be taken as the largest (in absolute value) eigenvalue of the Jacobian  $\partial f(u)/\partial u$ . The CFL number should be less than one for stability and in our computations it is taken to be between 0.1 and 0.6 (typically 0.4) depending on the stiffness of the cooling source term.

#### 4. ASTROPHYSICAL JET SIMULATIONS

Computational units for the supersonic jet simulations presented in the Figures are given in Table I. In these units,  $m_H = 1$ .

**Table I.** Computational Units for the Jets

Physical quantity	Basic scale
Length	$\bar{l} = 10^{11}$ km
Time	$\bar{t} = 10^{10}$ s
Velocity	$\bar{u} = 10$ km/s
Density	$\bar{\rho} = 100$ H/cm <sup>3</sup>
Energy density & pressure	$\bar{E} = \bar{P} = 104.4$ eV/cm <sup>3</sup>
Temperature	$\bar{T} = 1.044$ eV/ $k_B = 12,115$ K

The initial conditions were specified by ambient values for density, pressure, and temperature, except at the inflow boundary of the jet, where the density, pressure, and temperature were those of the jet. Through-flow boundary conditions were implemented by ghost points for the rest of the boundary. The timestep is controlled by the CFL factor, and the Mach 80 jet simulations required on the order of 2000 timesteps.

To validate the WENO-LF simulations, we made a comparison of simulations of a Mach 5 jet with results from LeVeque's software package CLAWPACK [25,26] (Conservation LAWs PACKage). CLAWPACK consists of routines for solving time-dependent nonlinear hyperbolic conservation laws based on higher order Godunov methods and (approximate) Riemann problem solutions, while the WENO-LF scheme does not directly employ Riemann problem solutions.

The simulations of the Mach 5 jets were performed on a  $300\Delta x \times 300\Delta y$  grid for WENO-LF (Fig. 1) and a  $200\Delta x \times 200\Delta y$  grid for CLAWPACK (Fig. 2). On a given grid, second-order CLAWPACK attains higher resolution of shocks for the jet problem than third-order WENO-LF, because CLAWPACK solves (approximate) Riemann problems. However WENO-LF with a  $300\Delta x \times 300\Delta y$  grid shows slightly higher resolution of the terminal and bow shocks and runs slightly faster than CLAWPACK with a  $200\Delta x \times 200\Delta y$  grid.

For the Mach 5 jets, the jet width is  $10^{10}$  km and the evolution time is  $4 \times 10^9$  s  $\approx 130$  yr. The Mach number of the jet inflow is Mach 1.7 with respect to the soundspeed in the light ambient gas and Mach 5.3 with respect to the soundspeed in the heavy jet gas. Excellent agreement was obtained between the two very different methods.

At Mach numbers above 6, the Roe Riemann solver in the current version of CLAWPACK fails, due to the generation of negative pressures in the Riemann solver around the rollup of the jet tip. With the HLLC Riemann solver and component-wise limiting (supplied by

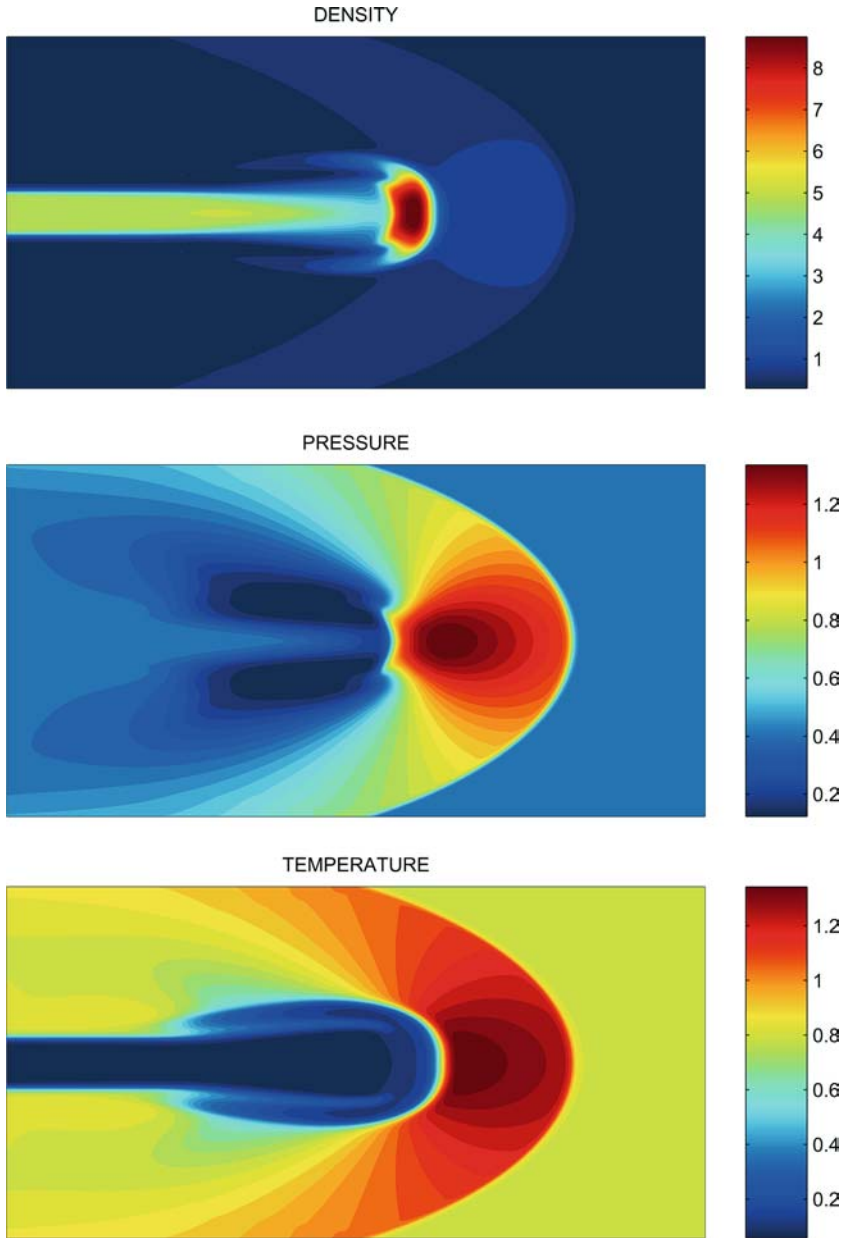


Fig. 1. WENO-LF simulation of Mach 5 jet.

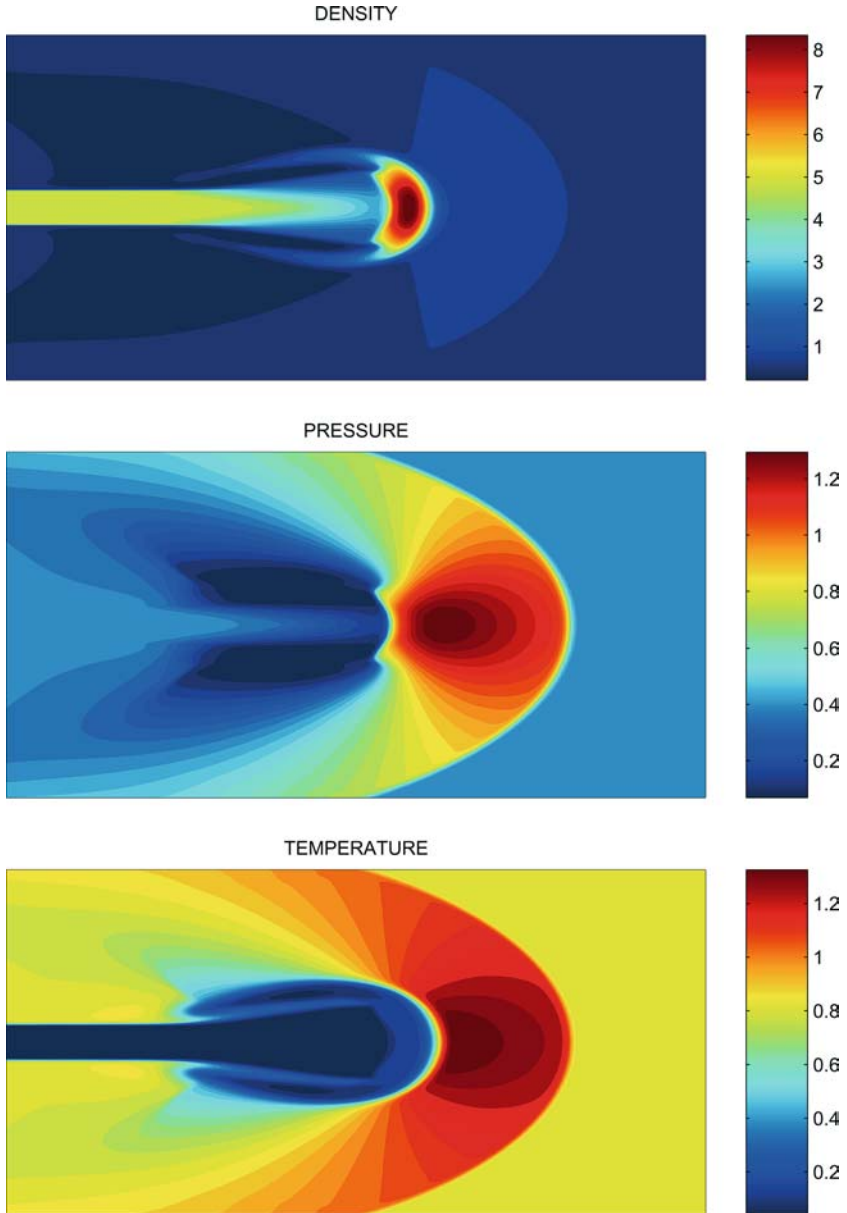


Fig. 2. CLAWPACK simulation of Mach 5 jet.

**Table II.** Parameters for the Jets in HH 1–2

Jet	Ambient
$\gamma = 5/3$	$\gamma = 5/3$
$\rho_j = 500 \text{ H/cm}^3$	$\rho_a = 50 \text{ H/cm}^3$
$u_j = 300 \text{ km/s}$	$u_a = 0$
$T_j = 1000 \text{ K}$	$T_a = 10,000 \text{ K}$
$c_j = 3.8 \text{ km/s}$	$c_a = 12 \text{ km/s}$

LeVeque), CLAWPACK can simulate the jets up to Mach 23. To reach Mach 80, a new (approximate) Riemann solver could perhaps be developed for CLAWPACK, but we chose instead to use the WENO-LF method.

The jets in HH 1–2 have the parameters listed in Table II. The simulations of the Mach 80 jets were performed with the WENO-LF method on a  $500\Delta x \times 250\Delta y$  grid. For the Mach 80 jets, the jet width is  $10^{10} \text{ km}$  and the evolution time is  $7 \times 10^8 \text{ s} \approx 22 \text{ yr}$ . The Mach number of the jet inflow is Mach 25 with respect to the soundspeed in the light ambient gas and Mach 80 with respect to the soundspeed in the heavy jet gas.

Our simulations with radiative cooling accurately reproduce the morphology and physics of the cylindrically symmetrical jet in HH 1–2, including the bow shock ahead of the jet, the terminal Mach disk just inside the tip of the jet, and the Kelvin–Helmholtz rollup of the jet tip. Note the differences between the Mach 80 jet without (Fig. 3) and with (Fig. 4) radiative cooling. The jet with radiative cooling has a much higher density contrast near the jet tip (as the shocked, heated gas cools radiatively, it compresses), a much thinner bow shock, reduced Kelvin–Helmholtz rollup of the jet tip, and a lower average temperature. The simulated shock speed  $u_s \approx 200 \text{ km/s}$ , and the simulated post-shock temperature  $T_\star \approx 500,000 \text{ K}$ , which agrees with the astrophysical formula

$$T_\star \approx 1.4 \times 10^5 \left( \frac{u_s}{100 \text{ km/s}} \right)^2 \text{ K.} \quad (19)$$

Radiative cooling is essential in understanding the density contrast and morphology of the jets and bow shocks in HH 1–2. Preliminary simulations indicate that we can reproduce the morphology of the asymmetrical jet if the simulated jet collides with an ambient blob of heavy gas (Fig. 5). In this simulation, a stationary blob of heavy gas with density

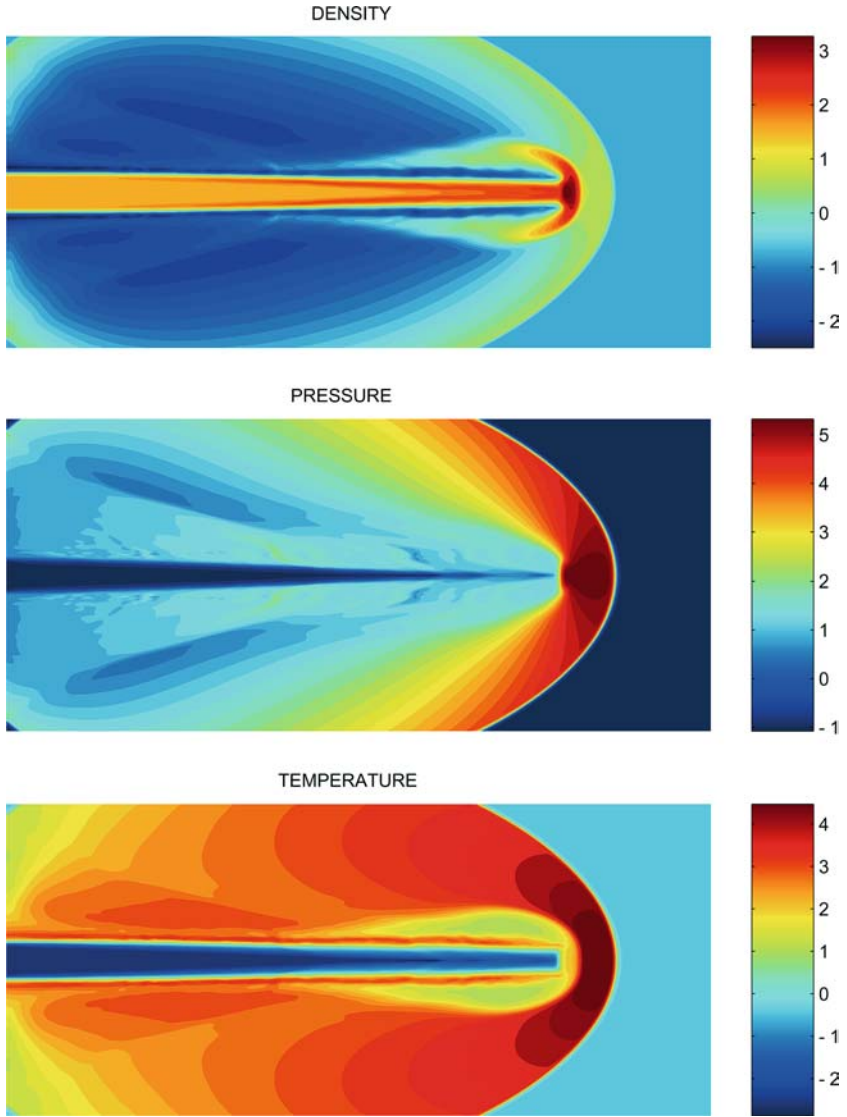
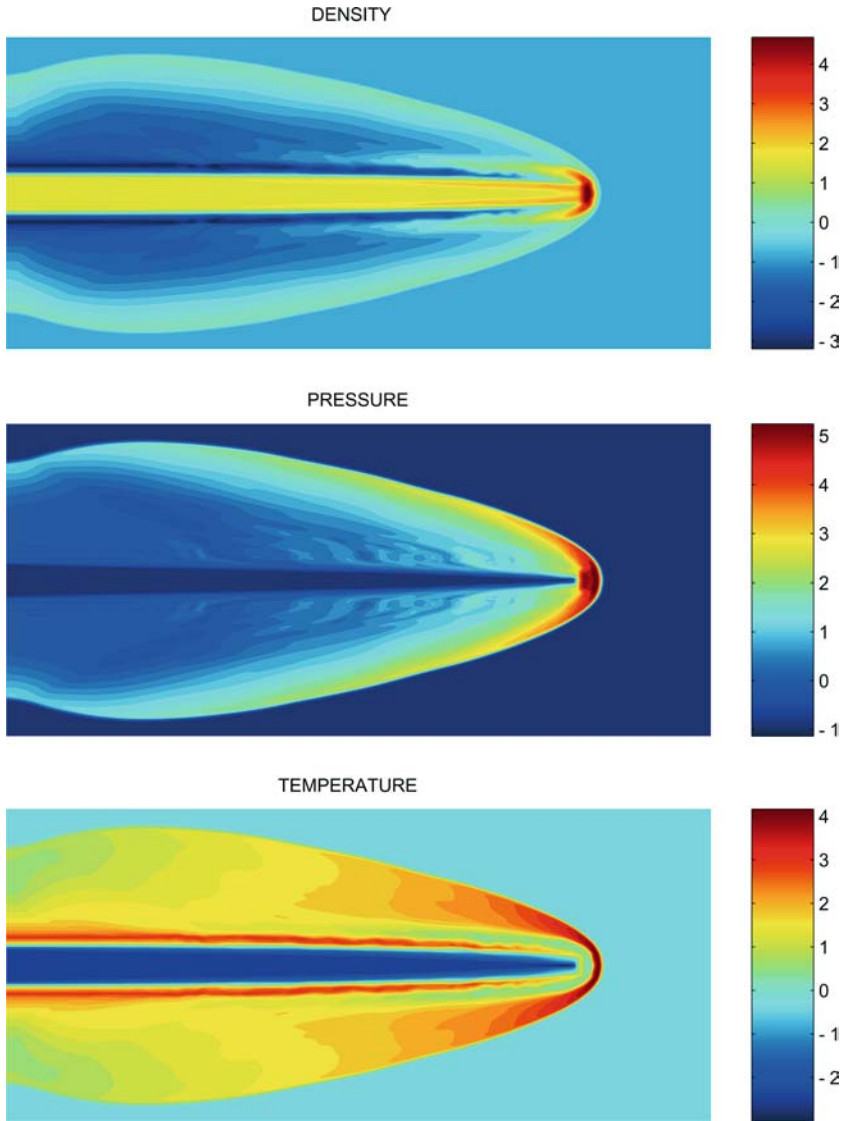


Fig. 3. Simulation of Mach 80 jet without radiative cooling. Scales are logarithmic.



**Fig. 4.** Simulation of Mach 80 jet with radiative cooling. Scales are logarithmic.

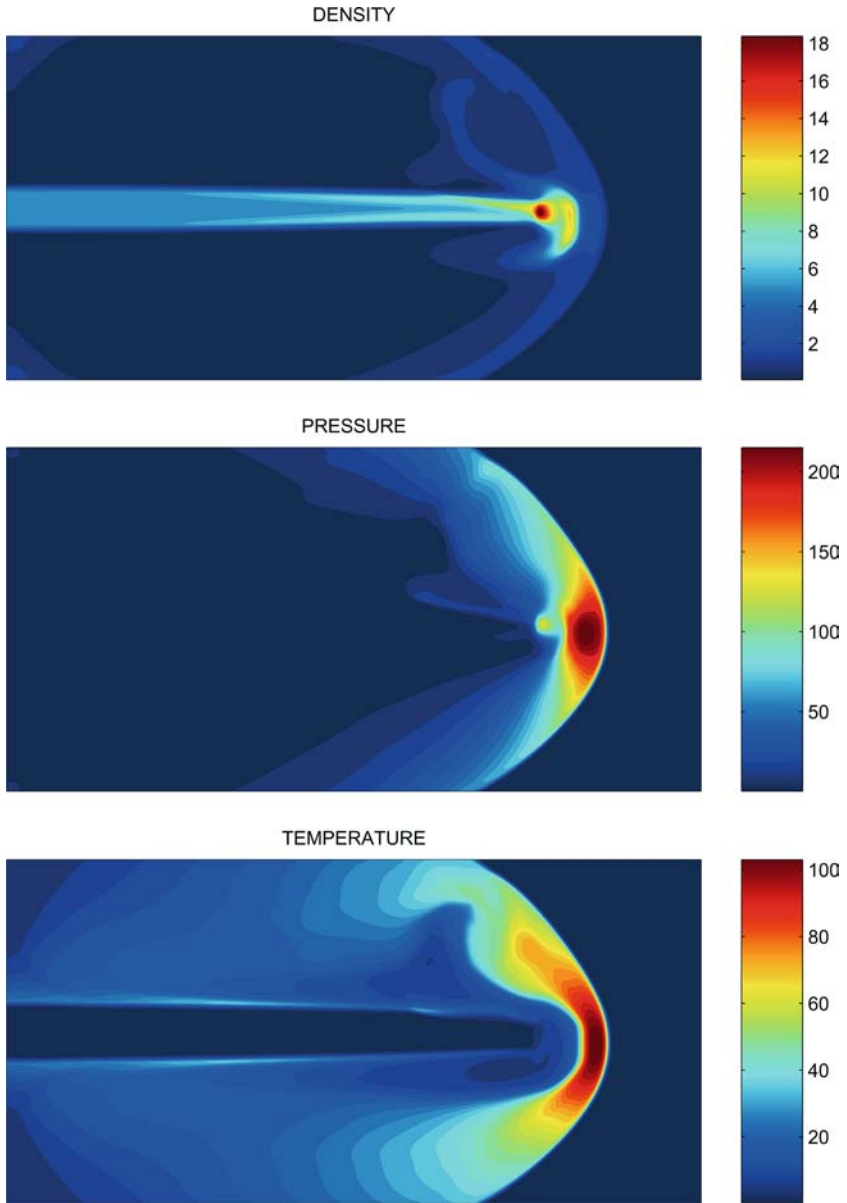


Fig. 5. Simulation of Mach 80 jet interacting with an ambient blob of gas.

and pressure equal to that of the jet was placed in the middle of the simulation region, slightly above the jet axis. Then the jet was allowed to propagate and interact with the blob.

## 5. CONCLUSION

The Euler equations have been applied here to very high temperature and pressure astrophysical jets, with the additional effects of radiative cooling. We believe the simulations are an excellent approximation to the physics of the jets, since viscosity is extremely small in the astrophysical setting, and the main corrections to the ideal gas approximation are included in the radiative cooling term.

In order to make a detailed comparison of the simulations and the astrophysical images of the HH 1–2 jets including reproducing morphology, shock structure, and temperature/ionization profiles of both jets, as well as the pathological features of the asymmetrical jet, we plan to simulate the interaction of the jets with their ambient environments in more detail and to extend the numerical code to a parallel version in three-dimensions. Three-dimensional simulations with moderate resolution are feasible on modern workstations. The parallel version is needed to achieve high resolution of fully 3D flows and shock structures.

## ACKNOWLEDGMENTS

We would like to thank Jeff Hester for valuable discussions. The authors would like to acknowledge for the following: (1) Research supported in part by the BK21 project at KAIST (Youngsoo Ha); (2) Research supported in part by the Space Telescope Science Institute under grant HST-GO-09863.06-A (Carl L. Gardner); (3) Research supported in part by the National Science Foundation under grant DMS-0107428. (Anne Gelb); (4) Research supported in part by the Army Research Office under grant DAAD19-00-1-0405 and in part by the National Science Foundation under grant DMS-0207451 (Chi-Wang Shu).

## REFERENCES

1. Shu, C.-W. (1999). High order ENO and WENO schemes for computational fluid dynamics, in *High-Order Methods for Computational Physics*, Lecture Notes in Computational Science and Engineering vol. 9, Springer Verlag, New York pp. 439–582.

2. Norman, M. L., Smarr, L. L., Winkler, K.-H. A. and Smith, M. D. (1982). Structure and dynamics of supersonic jets. *Astronomy and Astrophysics* **113**, 285–302.
3. Smarr, L. L., Norman, M. L., and Winkler, K.-H. A. (1984). Shocks, interfaces, and patterns in supersonic jets. *Physica D* **12**, 83.
4. Stone, J. M., and Norman, M. L. (1993). Numerical simulations of protostellar jets with nonequilibrium cooling. 1. Method and 2-dimensional results. *Astrophysical J.* **413**, 198–209.
5. Stone, J. M., and Norman, M. L. (1993). Numerical simulations of protostellar jets with nonequilibrium cooling. 2. Models of pulsed jets. *Astrophysical J.* **413**, 210–220.
6. Stone, J. M., and Norman, M. L. (1994.) Numerical simulations of protostellar jets with nonequilibrium cooling. 3. 3-dimensional results. *Astrophysical J.* **420**, 237–246.
7. Norman, M. L. (1990). Fluid-dynamics of astrophysical jets. *Ann. New York Acad. Sci.* **617**, 217–233.
8. Lee, C. F., Stone, J. M., Ostriker, E. C., and Mundy, L. G. (2001). Hydrodynamic simulations of jet- and wind-driven protostellar outflows. *Astrophysical J.* **557**, 429–442.
9. Gardner, C. L. (1986). Supersonic interface instabilities of accelerated surfaces and jets. *Phys. Fluids* **29**, 690–695.
10. Gardner, C. L., Glimm, J., McBryan, O., Menikoff, R., Sharp, D. H., and Zhang, Q. (1998). The dynamics of bubble growth for Rayleigh–Taylor unstable interfaces, *Phys. Fluids* **31**, 447–465.
11. Zhao, J. H., Burns, J. O., Norman, M. L., and Sulkanen, M. E. (1992). Instabilities in astrophysical jets. 2. numerical simulations of slab jets. *Astrophysical J.* **387**, 83.
12. Hardee, P. E., White, R. E., Norman, M. L., Cooper, M. A., and Clarke, D. A. (1992). Asymmetric morphology of the propagating jet. 2: The effect of atmospheric gradients. *Astrophysical J.* **387**, 460–483.
13. Hardee, P. E., and Stone, J. M. (1997). The stability of radiatively cooling jets. 1. Linear analysis. *Astrophysical J.* **483**, 121–135.
14. Stone, J. M., Xu, J. J., and Hardee, P. E. (1997). The stability of radiatively cooling jets. 2. Nonlinear evolution. *Astrophysical J.* **483**, 136.
15. Xu, J. J., Hardee, P. E., and Stone, J. M., (2000). The stability of radiatively cooled jets in three dimensions. *Astrophysical J.* **543**, 161–177.
16. Müller, E. (1988). Simulation of astrophysical fluid flow, in *Computational Methods for Astrophysical Fluid Flow*, Springer-Verlag, Berlin pp. 343–494.
17. Hester, J. J., Stapelfeldt, K. R., and Scowen, P. A., (1998). Hubble Space Telescope Wide Field Planetary Camera 2 observations of HH 1–2, *Astronomical J.* **116**, 372–395.
18. Schmutzler, T., and Tscharnuter, W. M. (1993). Effective radiative cooling in optically thin plasmas. *Astronomy and Astrophysics* **273**, 318–330.
19. Liu, X., Osher, S., and Chan, T., (1994). Weighted essentially non-oscillatory schemes. *J. Comput. Phys.* **115**, 200–212.
20. Jiang, G.-S., and Shu, C.-W. (1996). Efficient implementation of weighted ENO schemes. *J. Comput. Phys.* **126**, 202–228.
21. Balsara, D. and Shu, C.-W. (2000). Monotonicity preserving weighted essentially non-oscillatory schemes with increasingly high order of accuracy. *J. Comput. Phys.* **160**, 405–452.
22. Shu, C.-W. (1998). Essentially non-oscillatory and weighted essentially non-oscillatory schemes for hyperbolic conservation laws, In Cockburn, B., Johnson, C., Shu, C.-W., and Tadmor, E. (eds.), *Advanced Numerical Approximation of Nonlinear Hyperbolic Equations*. Lecture Notes in Mathematics, vol. 1697, Springer Verlag, New York pp. 325–432.
23. Shu, C.-W., and Osher, S., (1998). Efficient implementation of essentially non-oscillatory shock capturing schemes. *J. Comput. Phys.* **77**, 439–471.

24. Gottlieb, S., Shu, C.-W., and Tadmor, E. (2001). Strong stability preserving high order time discretization methods. *SIAM Review* **43**, 89–112.
25. <http://www.amath.washington.edu/~claw/>. R. J. LeVeque's *CLAWPACK website*.
26. LeVeque, R. J., (2002). *Finite Volume Methods for Hyperbolic Problems*. Cambridge: Cambridge University Press, Cambridge, UK